PERGAMON

Computers and Structures 75 (2000) 237–250

Computers & Structures

www.elsevier.com/locate/compstruc

A mixed-enhanced strain method Part I: Geometrically linear problems

Eric P. Kasper[a], Robert L. Taylor[b,*]

[a]Department of Civil and Environmental Engineering, California Polytechnic State University at San Luis Obispo, San Luis Obispo, CA 93407, USA

[b]Department of Civil and Environmental Engineering, University of California at Berkeley, Berkeley, CA 94720-1710, USA

Abstract

A general formulation of an assumed strain method in the context of mixed finite elements is presented. A mixed strain field is presented to which an enhancement is added resulting in a formulation which produces coarse mesh accuracy in bending dominated problems and locking-free response in the near incompressible limit. The structure of the mixed fields present permits a consistent variational stress recovery. Also, the construction of the formulation is such that the mixed parameters may be obtained explicitly and the resulting finite element arrays obtain full rank using standard order quadrature. In this paper our attention is restricted to the area of geometrically linear problems in solid mechanics. Specifically, we investigate the proposed formulation in the setting of nearly incompressible elasticity, physically nonlinear plasticity and thin shell structures. Representative simulations show favorable performance of the formulation.

Keywords: Mixed enhanced; Assumed strain; Finite element incompressibility; Plasticity

1. Introduction

It is known that finite elements based upon low order isoparametric displacement formulations exhibit poor performance in bending and locking in the nearly incompressible limit. Recent formulations which exhibit improved accuracy with respect to these two deficiencies fall into two categories namely *assumed stress* and *assumed strain* methods. The formulation presented herein is addressed in the context of *assumed strain* methods which have been preferred to their *assumed stress* counterparts, due to their natural compatibility with the strain drive format typically found in the algorithmic development of nonlinear materials.

One of the first developments in the area of *assumed strain* methods was by Wilson et al. [19], who proposed the addition of internal incompatible displacement modes of quadratic distribution to enhance bending performance of quadrilateral elements. Subsequently, it was discovered that the element failed the patch test for an arbitrary quadrilateral. Taylor et al. [15] proposed modifications to Wilson's original formulation which allowed for satisfaction of the patch test for arbitrary configurations. In later developments Simo and Rifai [10] present a systematic development of a class displacement method enhanced by *assumed strains*. They provided the framework for the development of low order elements possessing improved performance in bending dominate problems in the context of small strains. Issues related to convergence and stability were also presented. Further extensions were made to incorporate geometrically nonlinearities by

* Corresponding author.

0045-7949/00/$ - see front matter
PII: S0045-7949(99)00134-0

Simo and Armero [11], but was found to lock in the incompressible limit for three-dimensional (3D) hexagonal elements for both geometrically linear and nonlinear problems. Improvements were made for the 3D formulation by Simo et al. [12] which incorporated modifications to the tri-linear shape functions, additional enhanced modes and an increased quadrature rule. The resulting element yielded a locking-free response in the incompressible limit and improved bending characteristics for both geometrically linear and nonlinear problems. Andelfinger et al. [1] developed 2D and 3D enhanced strain elements for linear kinematics which overcome locking in the incompressible limit and behaved well in bending dominated regimes, but required a minimum of 21 element parameters for three dimensions. Weissman [18] also presented an enhanced formulation based on a three field functional which yield good performance for a wide class of problems using 15 element parameters. More recently, Korelc and Wriggers [4,5] developed 2D and 3D enhanced strain elements which yield favorable results, with only nine element parameters, thereby improving the efficiency of the element.

The approach of the present work utilizes a mixed finite element technique to overcome the difficulties which arise in the near incompressible limit and, simultaneously, enhance the resulting mixed strain field to improve coarse mesh accuracy in bending. Also, the formulation maintains a strain drive format such that general constitutive equations can be treated identically as in the Galerkin displacement finite element method. The approach is set forth by a reparameterization of the strain field in terms of a mixed approximation, from which a consistent formulation is derived. An additional enhancement is made to the strain field to improve the bending characteristics and give a locking-free response. The formulation is shown to have the appropriate convergence conditions as set forth in Ref. [10], namely consistency and stability. The element is formulated such that only standard order quadrature is needed for full rank, while maintaining a minimum number of element parameters, to achieve accurate results. The formulation also circumvents difficulties which can arise in *assumed strain* methods, for variational stress recovery.

The formulation of the strain field which appears in Ref. [10] and others differs from the present work in the reparameterization of both the stress and the strain field. As a consequence of their formulations, orthogonality conditions arise explicitly between the stress and enhanced strain field. This orthogonality condition makes full variational stress recovery difficult, if not impossible. The same orthogonality constraint exists implicitly in the present formulation, but due to the mixed construction of the stress field variational stress recovery is permissible.

The paper is outlined as follows. In Section 2, basic notation is given as well as the variational formulation for the model which is then cast into its weak form. Finite element interpolations are introduced in Section 3 along with the transformation relations for the mixed fields. The mixed-enhanced strain field and variationally consistent stress field recovery are developed and presented. The residual equations are then obtained from which a numerical formulation is presented. Representative numerical simulations for the case of plane strain and 3D elasticity are presented in Section 4, for linear kinematics with either elastic or elastic–plastic constitutive equations. Finally, in Section 5 conclusions are drawn and further work outlined.

2. Mixed-enhanced strain formulation

This section examines the proposed formulation in the setting of linear elasticity. We begin with an introduction of the basic notation used and then summarize a three-field Hu–Washizu functional in which the Dirichlet condition $\boldsymbol{u} = \bar{\boldsymbol{u}}$ on Γ_u is explicitly enforced. Finally, we present the resulting field equations in the weak form which is used subsequently for the finite element formulation.

2.1. Notation

The open set $\Omega \subset \mathbb{R}^n$ ($n = 1, 2$ or 3) with smooth boundary $\partial\Omega$ represents a bounded reference configuration $\mathscr{B}$ for the continuum body. We admit the decomposition of the boundary into two parts: $\Gamma_u \subset \partial\Omega$ where the displacement is prescribed as $\boldsymbol{u} = \bar{\boldsymbol{u}}$ and $\Gamma_t \subset \partial\Omega$ where the traction vector is prescribed as $\bar{\boldsymbol{t}} = \boldsymbol{\sigma n}$ subject to

$$\partial\Omega = \overline{\Gamma_u \cup \Gamma_t} \quad \text{and} \quad \Gamma_u \cap \Gamma_t = \varnothing \tag{2.1}$$

where $\boldsymbol{\sigma}$ is the stress tensor and $\boldsymbol{n}$ is the outward normal to the boundary.

The governing equations for linear elastostatics are given by the balance of linear and angular momentum

$$\mathrm{Div}[\boldsymbol{\sigma}] + \boldsymbol{b} = \boldsymbol{0} \tag{2.2a}$$

$$\boldsymbol{\sigma} = \boldsymbol{\sigma}^{\mathrm{T}} \tag{2.2b}$$

the strain–displacement relationship

$$\boldsymbol{\varepsilon} = \nabla^{(s)}\boldsymbol{u} = \frac{1}{2}\left(\nabla\boldsymbol{u} + \nabla\boldsymbol{u}^{\mathrm{T}}\right) \tag{2.3}$$

and for elastic stress response the constitutive equations

$$\boldsymbol{\sigma} = \frac{\partial W}{\partial \boldsymbol{\varepsilon}}. \tag{2.4}$$

In the above equation $\boldsymbol{\varepsilon}$ denotes the infinitesimal strain tensor, $\boldsymbol{\sigma}$ the stress tensor, $W(\boldsymbol{X}, \boldsymbol{\varepsilon})$ is a convex stored energy function, $\boldsymbol{b}$ is the body force per unit volume and Div [·] is the divergence operator.

For subsequent development let $\mathscr{U}$ be the space of admissible displacements written as

$$\mathscr{U} = \left\{ \boldsymbol{u}:\Omega \to \mathbb{R}^n | \boldsymbol{u} \in H^1(\Omega) \text{ and } \boldsymbol{u} = \bar{\boldsymbol{u}} \text{ on } \Gamma_u \right\} \tag{2.5}$$

while the space of admissible stresses and strains are denoted by $\mathscr{M}$

$$\mathscr{M} = \left\{ \boldsymbol{h}:\Omega \to \mathbb{R}^n \times \mathbb{R}^n | h_{ij} \in L^2(\Omega) \right\}. \tag{2.6}$$

2.2. Variational formulation

An approximate solution of the boundary value problem is constructed from a variational statement of the problem. The basic field equations may be included in a variational statement for the elasticity problem using a Hu–Washizu functional [17]. We use a special case of one such functional and examine its implications. Accordingly, we have a functional in which the displacement field, $\boldsymbol{u} \in \mathscr{U}$ the stress tensor, $\tilde{\boldsymbol{\sigma}} \in \mathscr{M}$ and the strain tensor, $\tilde{\boldsymbol{\varepsilon}} \in M$ are regarded as the independent variables. The proposed three-field functional $\Pi:\mathscr{U} \times \mathscr{M} \times \mathscr{M} \to \mathbb{R}$ may be expressed as

$$\Pi(\boldsymbol{u}, \tilde{\boldsymbol{\varepsilon}}, \tilde{\boldsymbol{\sigma}}) = \int_\Omega \left[W(\boldsymbol{X}, \tilde{\boldsymbol{\varepsilon}}) + \tilde{\boldsymbol{\sigma}}:(\boldsymbol{\varepsilon} - \tilde{\boldsymbol{\varepsilon}}) \right] \mathrm{d}V + \Pi_{\text{ext}}(\boldsymbol{u}) \tag{2.7}$$

where for conservative external loading

$$\Pi_{\text{ext}}(\boldsymbol{u}) = -\int_\Omega \boldsymbol{b} \cdot \boldsymbol{u} \, \mathrm{d}V - \int_{\Gamma_t} \bar{\boldsymbol{t}} \cdot \boldsymbol{u} \, \mathrm{d}S. \tag{2.8}$$

We may state the solution of Eq. (2.7) as: find $\boldsymbol{u}$, $\tilde{\boldsymbol{\varepsilon}}$ and $\tilde{\boldsymbol{\sigma}}$, with $\boldsymbol{u} \in \mathscr{U}$ for all admissible variations $\delta\boldsymbol{u} \in \mathscr{V}$, $\delta\tilde{\boldsymbol{\varepsilon}} \in \mathscr{M}$ and $\delta\tilde{\boldsymbol{\sigma}} \in \mathscr{M}$ which make the Hu–Washizu functional $\Pi(\boldsymbol{u}, \tilde{\boldsymbol{\varepsilon}}, \tilde{\boldsymbol{\sigma}})$ stationary, where $\mathscr{V}$ is the space of admissible variations in the displacement written as

$$\mathscr{V} = \left\{ \delta\boldsymbol{u}:\Omega \to \mathbb{R}^n | \delta\boldsymbol{u} \in H^1(\Omega) \text{ and } \delta\boldsymbol{u} = \boldsymbol{0} \text{ on } \Gamma_u \right\}. \tag{2.9}$$

Since there are no explicit constraints on $\tilde{\boldsymbol{\varepsilon}}$ and $\tilde{\boldsymbol{\sigma}}$ we may take the variations $\delta\tilde{\boldsymbol{\varepsilon}}$ and $\delta\tilde{\boldsymbol{\sigma}}$ to be contained within $\mathscr{M}$ as defined in Eq. (2.6).

The stationary point of Π is obtained by setting to zero the first variation of Eq. (2.7) with respect to the three independent fields. Accordingly

$$\int_\Omega \delta\boldsymbol{\varepsilon} \cdot \tilde{\boldsymbol{\sigma}} \, \mathrm{d}V - \int_\Omega \delta\boldsymbol{u} \cdot \boldsymbol{b} \, \mathrm{d}V - \int_{\Gamma_t} \delta\boldsymbol{u} \cdot \bar{\boldsymbol{t}} \, \mathrm{d}S = 0 \tag{2.10a}$$

$$\int_\Omega \delta\tilde{\boldsymbol{\varepsilon}} \cdot \left(\frac{\partial W}{\partial \tilde{\boldsymbol{\varepsilon}}} - \tilde{\boldsymbol{\sigma}} \right) \mathrm{d}V = 0 \text{ in } \Omega \tag{2.10b}$$

$$\int_\Omega \delta\tilde{\boldsymbol{\sigma}} \cdot (\boldsymbol{\varepsilon} - \tilde{\boldsymbol{\varepsilon}}) \, \mathrm{d}V = 0. \tag{2.10c}$$

for all admissible variations $\delta\boldsymbol{u} \in \mathscr{V}$, $\delta\tilde{\boldsymbol{\varepsilon}} \in \mathscr{M}$ and $\delta\tilde{\boldsymbol{\sigma}} \in \mathscr{M}$.

3. Finite element approximations

In this section we outline the interpolates used for the field variables, from which the mixed strain and stress fields are constructed in terms of nodal parameters as well as internal element parameters. Using the mixed strain field we construct an approximation to the three-field variational formulation. We then use the stationary condition to yield a reduced set of nonlinear equations, which are then linearized. From these equations finite element arrays are formulated. Finally, we outline a procedure for implementation of the formulation.

3.1. Finite element interpolations for the field variables

We begin by a discretization of the given reference domain Ω into a collection of polygonal shaped subdomains, $\bar{\Omega}_e$, such that $\Omega \approx \Omega^h = \bigcup_e \bar{\Omega}_e$ where $\bar{\Omega}_e$ is the closure of an individual element. Note that the collection is an approximation of the actual domain Ω. We admit the decomposition of the approximation to the boundary as $\partial\Omega \approx \partial\Omega^h = \overline{\Gamma_u^h \cup \Gamma_t^h}$ and $\Gamma_u^h \cap \Gamma_t^h = \varnothing$.

For isoparametric finite elements we define the reference geometry $\mathbf{X}^h \in \mathbb{R}^n$ and displacement field $\mathbf{u}^h \in \mathscr{U}^h$ over a typical element $\bar{\Omega}_e$ in the form

$$\mathbf{X}^h = \sum_{I=1}^{nen} N_I(\boldsymbol{\xi}) \hat{\mathbf{X}}^I \quad \text{and} \quad \mathbf{u}^h = \sum_{I=1}^{nen} N_I(\boldsymbol{\xi}) \hat{\mathbf{u}}^I, \tag{3.1}$$

where $N_I(\boldsymbol{\xi})$ are the standard isoparametric shape functions associated with node I, *nen* is the number of nodes on element $\bar{\Omega}_e$, h is a characteristic length of element $\bar{\Omega}_e$ and $\hat{\mathbf{u}}^h$, $\hat{\mathbf{X}}^h \in \mathbb{R}^n$, see Refs. [3,21] for further details.

For the approximate problem we introduce the space $\mathscr{U}^h$ as a finite-dimensional approximation of $\mathscr{U}$, accordingly the space of admissible displacement fields maybe written as

$$\mathscr{U}^h = \left\{ \mathbf{u}^h | \mathbf{u}^h \in H^1(\Omega^h) \text{ and } \mathbf{u}^h = \bar{\mathbf{u}}^h \text{ on } \Gamma_u^h \right\}. \tag{3.2}$$

Lastly, the space $\mathscr{M}^h$, which contains the approximations to the stress and strain fields, is a finite-dimensional approximation of $\mathscr{M}$ given by

$$\mathscr{M}^h = \left\{ \boldsymbol{h}^h | h^h_{ij} \in L^2(\Omega^h) \right\}. \tag{3.3}$$

3.1.1. Mixed quantities

The key idea for the mixed stress and strain fields is to develop the interpolates in the natural or isoparametric space and transform the results to the physical space. Based on requirements of tensor calculus [14], we use the following transformation relations for the stress and strain tensors

$$\begin{aligned} &\mathscr{S}_{\alpha\beta}(\boldsymbol{\xi}, \boldsymbol{\beta}) = \tilde{\boldsymbol{\sigma}}_{IJ}(\boldsymbol{T}_{I\alpha})^{-1}\left(\boldsymbol{T}_{J\beta}\right)^{-1} \quad \text{and} \\ &\mathscr{E}_{\alpha\beta}(\boldsymbol{\xi}, \boldsymbol{\beta}) = \tilde{\boldsymbol{\varepsilon}}_{IJ}\boldsymbol{T}_{I\alpha}\boldsymbol{T}_{J\beta} \end{aligned} \tag{3.4}$$

where $\mathscr{S}$ and $\mathscr{E}$ are the stress and strain in the isoparametric space, respectively. The above are defined so that $\mathscr{S}:\mathscr{E} = \tilde{\boldsymbol{\sigma}}:\tilde{\boldsymbol{\varepsilon}}$.

Let $\square$ denote the parent domain in the isoparametric space $\boldsymbol{\xi}$. Utilizing the mapping $\boldsymbol{X}:\square \to \Omega_e$: the Jacobian is expressed as

$$J_{I\alpha}(\boldsymbol{\xi}) = \frac{\partial X^I}{\partial \xi^\alpha} \quad \text{and} \quad j = \det J_{I\alpha}. \tag{3.5}$$

For the present paper the Jacobian used in Eq. (3.4) is averaged over the element Ω_e and used to define $\boldsymbol{T}$. This will permit direct inclusion of constant states, minimize the order of quadrature needed to evaluate the residual and tangent arrays and also eliminate problems associated with initially distorted elements. The average is denoted as

$$\boldsymbol{T} = \frac{1}{\Omega_e}\int_{\Omega_e} \boldsymbol{J}(\boldsymbol{\xi})\, \mathrm{d}V := \boldsymbol{J}_{\text{avg}}. \tag{3.6}$$

Substituting Eq. (3.6) into Eq. (3.4) yields the transformation of the fields $(\mathscr{S}, \mathscr{E})$ in the isoparametric space to the fields $(\tilde{\boldsymbol{\sigma}}, \tilde{\boldsymbol{\varepsilon}})$ in the physical space

$$\mathscr{S}(\boldsymbol{\xi}, \boldsymbol{\beta}) = \boldsymbol{T}^{-1}\tilde{\boldsymbol{\sigma}}\boldsymbol{T}^{-\mathrm{T}} \quad \text{and} \quad \mathscr{E}(\boldsymbol{\xi}, \boldsymbol{\gamma}) = \boldsymbol{T}^{\mathrm{T}}\tilde{\boldsymbol{\varepsilon}}\boldsymbol{T}. \tag{3.7}$$

Remark 3.1.

1. Alternatively, the Jacobian can be evaluated at the centroid, as originally suggested by Pian and Sumihara [9] and Taylor et al. [15].
2. Since the above transformation relations for the stress and strain are typically a measure of the isoparametric and physical space, alternative transformations are admissible. Numerical observation by Glaser and Armero [2] and Wriggers and Reese [20] confirmed during the developments of the present work show that replacing $\boldsymbol{J}$ by $\boldsymbol{J}^{-\mathrm{T}}$ or $\boldsymbol{J}^{\mathrm{T}}$ may result in transformation relations which are superior for the class of problems examined.

We assume there exist linear maps $\mathscr{E}_1(\boldsymbol{\xi}, \cdot)$ and $\mathscr{E}_2(\boldsymbol{\xi}, \cdot)$ for which the fields $(\mathscr{S}, \mathscr{E})$ in the isoparametric space may be expressed as:

$$\mathscr{S}(\boldsymbol{\xi}, \boldsymbol{\beta}) = \hat{\boldsymbol{\beta}}_0 + \mathscr{E}_1(\boldsymbol{\xi}, \boldsymbol{\beta}) \tag{3.8a}$$

$$\mathscr{E}(\boldsymbol{\xi}, \boldsymbol{\gamma}) = \hat{\boldsymbol{\gamma}}_0 + \frac{1}{j}\left[\mathscr{E}_1(\boldsymbol{\xi}, \boldsymbol{\gamma}) + \mathscr{E}_2(\boldsymbol{\xi}, \boldsymbol{\alpha})\right] \tag{3.8b}$$

where $\hat{\boldsymbol{\beta}}_0$, $\boldsymbol{\beta}$, $\hat{\boldsymbol{\gamma}}_0$ and $\boldsymbol{\gamma}$ are parameters; and $\mathscr{E}_1(\boldsymbol{\xi}, \boldsymbol{\gamma})$ and $\mathscr{E}_2(\boldsymbol{\xi}, \boldsymbol{\alpha})$ denote linear forms

$$\begin{aligned} &\mathscr{E}_1(\boldsymbol{\xi}, \boldsymbol{\gamma}) = \sum_{k=1}^{n} \mathscr{E}_{k1}(\boldsymbol{\xi})\boldsymbol{\gamma}_k \quad \text{and} \\ &\mathscr{E}_2(\boldsymbol{\xi}, \boldsymbol{\alpha}) = \sum_{k=1}^{m} \mathscr{E}_{k2}(\boldsymbol{\xi})\boldsymbol{\alpha}_k \end{aligned} \tag{3.9}$$

where n and m are the number of parameters for the mixed and enhanced fields, respectively.

We construct the approximations $\mathscr{E}_1$ and $\mathscr{E}_2$ such that

$$\int_{\square} \mathscr{E}_1(\,\cdot\,)\, \mathrm{d}\square = 0, \tag{3.10a}$$

$$\int_{\square} \mathscr{E}_2(\,\cdot\,)\, \mathrm{d}\square = 0 \tag{3.10b}$$

and

$$\int_{\square} \mathscr{E}_1(\,\cdot\,)\mathscr{E}_2(\,\cdot\,)\, \mathrm{d}\square = 0. \tag{3.10c}$$

The relations in Eqs. (3.10a)–(3.10c) will be used subsequently to decouple and solve for the element parameters of the mixed stress and strain.

Remark 3.2.

1. The mapping $\mathscr{E}_2(\boldsymbol{\xi}, \boldsymbol{\alpha})$ with its associated element parameters, $\boldsymbol{\alpha}$ were added to Eq. (3.8b) for two reasons: (a) to improve performance in nearly incompressible regions, and (b) to improve coarse mesh accuracy in bending dominated regimes.
2. Note the strain field in Eqs. (3.8a) and (3.8b) has more parameters than the stress, hence, we adopt

Table 1
Two-dimensional interpolations

i	j	$[\mathscr{E}_1(\boldsymbol{\varepsilon}, \boldsymbol{\gamma})]_{ij}$	$[\mathscr{E}_2(\boldsymbol{\xi}, \boldsymbol{\alpha})]_{ij}$
1	1	$\xi_2\gamma_1$	$\xi_1\alpha_1$
2	2	$\xi_1\gamma_2$	$\xi_2\alpha_2$
1	2	0	0

the phrase mixed-enhanced strain as an extension of the terminology introduced by Simo and Rifai [10].

For 2D and 3D problems employing four-node quadrilateral and eight-node hexahedral elements the maps $\mathscr{E}_1(\boldsymbol{\xi}, \cdot)$ and $\mathscr{E}_2(\boldsymbol{\xi}, \cdot)$ are given in Tables 1 and 2, respectively. Noting symmetry, the independent components are ordered in standard Voigt notation as given in Tables 1 and 2.

In both cases the minimum number of parameters needed to obtain proper rank of the mixed formulation are used to define $\mathscr{E}_1(\boldsymbol{\xi}, \cdot)$.

The interpolates for $\tilde{\boldsymbol{\sigma}}$ and $\tilde{\boldsymbol{\varepsilon}}$ in the physical space are obtained by equating Eqs. (3.7), (3.8a) and (3.8b), resulting in

$$\tilde{\boldsymbol{\sigma}} = \boldsymbol{\beta}_0 + \boldsymbol{T}\mathscr{E}_1(\boldsymbol{\xi}, \boldsymbol{\beta})\boldsymbol{T}^{\mathrm{T}} \tag{3.11a}$$

$$\tilde{\boldsymbol{\varepsilon}} = \boldsymbol{\gamma}_0 + \frac{1}{j}\boldsymbol{T}^{-\mathrm{T}}\big[\mathscr{E}_1(\boldsymbol{\xi}, \boldsymbol{\gamma}) + \mathscr{E}_2(\boldsymbol{\xi}, \boldsymbol{\alpha})\big]\boldsymbol{T}^{-1} \tag{3.11b}$$

where the reparameterization of the constant terms is given by

$$\boldsymbol{\beta}_0 = \boldsymbol{T}\hat{\boldsymbol{\beta}}_0\boldsymbol{T}^{\mathrm{T}} \quad \text{and} \quad \boldsymbol{\gamma}_0 = \boldsymbol{T}^{-\mathrm{T}}\hat{\boldsymbol{\gamma}}_0\boldsymbol{T}^{-1}. \tag{3.12}$$

Remark 3.3. Note the enhanced parameters added in Table 2 for the normal strain components are chosen such that the resulting strain components are complete polynomials. This is done to provide the necessary equations to enforce the incompressibility constraint without loss of rank for the resulting finite element arrays, see Ref. [12].

Table 2
Three-dimensional interpolations

i	j	$[\mathscr{E}_1(\boldsymbol{\xi}, \boldsymbol{\gamma})]_{ij}$	$[\mathscr{E}_2(\boldsymbol{\xi}, \boldsymbol{\alpha})]_{ij}$
1	1	$\xi_2\gamma_1 + \xi_3\gamma_2 + \xi_2\xi_3\gamma_3$	$\xi_1\alpha_1 + \xi_1\xi_2\alpha_2 + \xi_1\xi_3\alpha_3$
2	2	$\xi_1\gamma_4 + \xi_3\gamma_5 + \xi_1\xi_3\gamma_6$	$\xi_2\alpha_4 + \xi_2\xi_3\alpha_5 + \xi_1\xi_2\alpha_6$
3	3	$\xi_1\gamma_7 + \xi_2\gamma_8 + \xi_1\xi_2\gamma_9$	$\xi_3\alpha_7 + \xi_2\xi_3\alpha_8 + \xi_1\xi_3\alpha_9$
1	2	$\xi_3\gamma_{10}$	0
2	3	$\xi_1\gamma_{11}$	0
1	3	$\xi_2\gamma_{12}$	0

3.2. Mixed-enhanced strain field

By isolating Eq. (2.10c) we may express the element parameters appearing in the mixed-enhanced strain, $\tilde{\boldsymbol{\varepsilon}}$ in terms of the nodal displacement parameters $\hat{\boldsymbol{u}}^I$. Recall Eq. (2.10c)

$$\int_\Omega \mathrm{tr}\big[\delta\tilde{\boldsymbol{\sigma}}^{\mathrm{T}}(\boldsymbol{\varepsilon} - \tilde{\boldsymbol{\varepsilon}})\big]\,\mathrm{d}V = 0. \tag{3.13}$$

Substituting Eqs. (3.11a) and (3.11b) into Eq. (3.13) and noting Eqs. (3.10a)–(3.10c) we arrive at

$$\int_\Omega \mathrm{tr}\Big[\delta\boldsymbol{\beta}_0^{\mathrm{T}}(\boldsymbol{\varepsilon} - \boldsymbol{\gamma}_0)\Big]\,\mathrm{d}V = 0 \tag{3.14a}$$

$$\int_\Omega \mathrm{tr}\left[\mathscr{E}_1^{\mathrm{T}}(\delta\boldsymbol{\beta})\left(\boldsymbol{T}^{\mathrm{T}}(\boldsymbol{\varepsilon} - \boldsymbol{\gamma}_0)\boldsymbol{T} - \frac{1}{j}\mathscr{E}_1(\boldsymbol{\gamma})\right)\right]\mathrm{d}V = 0. \tag{3.14b}$$

Since $\delta\boldsymbol{\beta}_0$ and $\delta\boldsymbol{\beta}$ are independent of the arguments within the integrand and the limits of integration, we obtain $\boldsymbol{\gamma}_0$ as

$$\boldsymbol{\gamma}_0 = \frac{1}{V}\int_\Omega \boldsymbol{\varepsilon}\,\mathrm{d}V := \boldsymbol{\varepsilon}_0 \tag{3.15}$$

and cast Eq. (3.14b) as

$$\int_\Omega \bar{\boldsymbol{E}}_1^{\mathrm{T}}\left(\boldsymbol{E}_3\boldsymbol{u} - \frac{1}{j}\boldsymbol{E}_1\boldsymbol{\gamma}\right)\mathrm{d}V = 0. \tag{3.16}$$

In Eq. (3.16) we have defined the following operators which enable a mapping between tensors and matrices

$$\begin{aligned} &\mathscr{E}_1(\boldsymbol{\gamma}) \rightarrow \boldsymbol{E}_1\boldsymbol{\gamma}, \quad \mathscr{E}_1(\boldsymbol{\beta}) \rightarrow \bar{\boldsymbol{E}}_1\boldsymbol{\beta}, \\ &\boldsymbol{T}^{\mathrm{T}}(\boldsymbol{\varepsilon} - \boldsymbol{\varepsilon}_0)\boldsymbol{T} \rightarrow \boldsymbol{E}_3\boldsymbol{u}. \end{aligned} \tag{3.17}$$

For two dimensions

$$\boldsymbol{E}_1 = \begin{bmatrix} \xi_2 & 0 \\ 0 & \xi_1 \\ 0 & 0 \end{bmatrix} \quad \text{and} \quad \bar{\boldsymbol{E}}_1 = \begin{bmatrix} \xi_2 & 0 \\ 0 & \xi_1 \\ 0 & 0 \end{bmatrix}. \tag{3.18}$$

Grouping terms in Eq. (3.16) and solving for the element parameter $\boldsymbol{\gamma}$ gives

$$\boldsymbol{\gamma} = \boldsymbol{G}^{-1}\boldsymbol{g}\boldsymbol{u} = \boldsymbol{b}\boldsymbol{u} \tag{3.19}$$

where

$$\boldsymbol{g} = \int_{\Omega} \bar{\boldsymbol{E}}_1^{\mathrm{T}} \boldsymbol{E}_3 \, \mathrm{d}V \quad \text{and} \quad \boldsymbol{G} = \int_{\square} \bar{\boldsymbol{E}}_1^{\mathrm{T}} \boldsymbol{E}_1 \, \mathrm{d}\square. \tag{3.20}$$

Using Eqs. (3.15) and (3.19), we may rewrite Eq. (3.11b) in matrix notation as

$$\tilde{\boldsymbol{\varepsilon}} = \boldsymbol{B}_u(\boldsymbol{\xi})\boldsymbol{u} + \boldsymbol{B}_\alpha(\boldsymbol{\xi})\boldsymbol{\alpha}. \tag{3.21}$$

Remark 3.4.

1. Using the interpolations in Tables 1 and 2 results in a diagonal form for $\boldsymbol{G}$. This simplifies the solution of the element parameters $\boldsymbol{\gamma}$ to a set of scalar decoupled equations.
2. Note orthogonality of $\mathscr{E}_1$ and $\mathscr{E}_2$ is assumed by Eq. (3.10c). In Appendix A we present an alternative formulation for constructing $\mathscr{E}_1$ and $\mathscr{E}_2$, which satisfy the orthogonality condition. However, Eqs. (3.10a) and (3.10b) may not hold in general.
3. The distinction between $\boldsymbol{E}_1$ and $\bar{\boldsymbol{E}}_1$ arises, since the array $\boldsymbol{E}_1$ associated with the strain will have two's which multiply the shear coefficients (for the 3D case).
4. From the condition (3.10b) the resulting enhanced strain displacement matrix $\boldsymbol{B}_\alpha$, will inherit the same properties provided any operators multiplying it are constant, $\int_\Omega \boldsymbol{B}_\alpha \boldsymbol{A}_0 \, \mathrm{d}V = 0$ with $\boldsymbol{A}_0 = \text{constant}$. Thus, the consistency condition or patch test set forth in Ref. [10] is satisfied.
5. The stability condition set forth in Ref. [10] requires that the conforming and enhanced spaces be independent. This is satisfied by the choice of interpolations found in Tables 1 and 2, i.e., the mappings are disjoint.

3.3. Variational stress recovery

By isolating Eq. (2.10b) we may solve for the element parameters of the mixed stress, $\tilde{\boldsymbol{\sigma}}$. Recall Eq. (2.10b)

$$\int_{\Omega} \delta\tilde{\boldsymbol{\varepsilon}} \cdot (\boldsymbol{\sigma} - \tilde{\boldsymbol{\sigma}}) \, \mathrm{d}V = 0 \tag{3.22}$$

where

$$\boldsymbol{\sigma} = \frac{\partial W}{\partial \tilde{\boldsymbol{\varepsilon}}} \tag{3.23}$$

Substituting Eqs. (3.11a) and (3.11b) into Eq. (3.22) and noting Eqs. (3.10a)–(3.10c) we arrive at

$$\int_{\Omega} \mathrm{tr}\Big[\delta\boldsymbol{\gamma}_0^{\mathrm{T}}\big(\boldsymbol{\sigma} - \boldsymbol{\beta}_0\big)\Big] \, \mathrm{d}V = 0 \tag{3.24a}$$

$$\int_{\Omega} \mathrm{tr}\left[\frac{1}{j}\mathscr{E}_1^{\mathrm{T}}(\delta\boldsymbol{\gamma})\Big(\boldsymbol{T}^{-1}\big(\boldsymbol{\sigma} - \boldsymbol{\beta}_0\big)\boldsymbol{T}^{-\mathrm{T}} - \mathscr{E}_1(\boldsymbol{\beta})\Big)\right] \mathrm{d}V = 0. \tag{3.24b}$$

Regarding $\delta\boldsymbol{\gamma}_0$ and $\delta\boldsymbol{\gamma}$ as independent of the arguments within the integrand and the limits of integration we may obtain $\boldsymbol{\beta}_0$ as

$$\boldsymbol{\beta}_0 = \frac{1}{V}\int_{\Omega} \boldsymbol{\sigma} \, \mathrm{d}V := \boldsymbol{\sigma}_0 \tag{3.25}$$

and cast Eq. (3.24b) as

$$\int_{\Omega} \frac{1}{j}\boldsymbol{E}_1^{\mathrm{T}}\big\{\boldsymbol{E}_5 - \bar{\boldsymbol{E}}_1\boldsymbol{\beta}\big\} \, \mathrm{d}V = 0 \tag{3.26}$$

where we have defined the following operators which enable a mapping between tensors and matrices

$$\boldsymbol{T}^{-1}(\boldsymbol{\sigma} - \boldsymbol{\sigma}_0)\boldsymbol{T}^{-\mathrm{T}} \rightarrow \boldsymbol{E}_5. \tag{3.27}$$

Grouping terms in Eq. (3.26) and solving for the element parameter $\boldsymbol{\beta}$ gives

$$\boldsymbol{\beta} = \boldsymbol{G}^{-1}\boldsymbol{h} \quad \text{where} \quad \boldsymbol{h} = \int_{\Omega} \frac{1}{j}\boldsymbol{E}_1^{\mathrm{T}}\boldsymbol{E}_5 \, \mathrm{d}V. \tag{3.28}$$

The variationally recoverable stress becomes

$$\tilde{\boldsymbol{\sigma}} = \boldsymbol{\beta}_0 + \boldsymbol{T}\mathscr{E}_1(\boldsymbol{\xi}, \boldsymbol{\beta})\boldsymbol{T}^{\mathrm{T}}. \tag{3.29}$$

Remark 3.5. The variational stresses developed above are used for postprocessing only and are not needed for the construction of the residual or tangent.

3.4. Residual and tangent

By construction, the substitution of Eq. (3.21) into Eq. (2.7) renders the second term of Eq. (2.7) zero, hence, we may express a modified functional $\hat{\Pi}$ as

$$\hat{\Pi}(\boldsymbol{u}, \tilde{\boldsymbol{\varepsilon}}) = \int_{\Omega} W(\tilde{\boldsymbol{\varepsilon}}) \, \mathrm{d}V + \Pi_{\mathrm{ext}}(\boldsymbol{u}) \tag{3.30}$$

The stationary condition of $\hat{\Pi}$ yields a reduced set of nonlinear equations, which may be expressed as

$$\delta\hat{\Pi} = \int_{\Omega} \frac{\partial W}{\partial \tilde{\boldsymbol{\varepsilon}}} : \delta\tilde{\boldsymbol{\varepsilon}} \, \mathrm{d}V \Longrightarrow \quad \big\{\, \delta\boldsymbol{u}^{\mathrm{T}} \quad \delta\boldsymbol{\alpha}^{\mathrm{T}} \,\big\} \int_{\Omega} \begin{Bmatrix} \boldsymbol{B}_u^{\mathrm{T}} \\ \boldsymbol{B}_\alpha^{\mathrm{T}} \end{Bmatrix} \boldsymbol{\sigma} \, \mathrm{d}V + \delta\Pi_{\mathrm{ext}} = 0 \tag{3.31}$$

where $\boldsymbol{\sigma}$ is defined in Eq. (3.23).

To solve the mixed boundary value problem the

above nonlinear equations are linearized and solved by a Newton's method as a sequence of linearized problems. Hence, linearizing Eq. (3.31) we obtain

$$d(\delta\hat{\Pi}) = \int_\Omega d\tilde{\boldsymbol{\varepsilon}}:\frac{\partial^2 W}{\partial\tilde{\boldsymbol{\varepsilon}}^2}:\delta\tilde{\boldsymbol{\varepsilon}}\,\mathrm{d}V \Longrightarrow$$
$$\left\{\delta\boldsymbol{u}^{\mathrm{T}} \quad \delta\boldsymbol{\alpha}^{\mathrm{T}}\right\}\int_\Omega\begin{bmatrix}\boldsymbol{K}_{uu} & \boldsymbol{K}_{u\alpha}\\ \boldsymbol{K}_{\alpha u} & \boldsymbol{K}_{\alpha\alpha}\end{bmatrix}\mathrm{d}V\begin{Bmatrix}d\boldsymbol{u}\\ d\boldsymbol{\alpha}\end{Bmatrix} \tag{3.32}$$

where

$$\boldsymbol{K}_{uu} = \boldsymbol{B}_u^{\mathrm{T}}\mathbb{D}\boldsymbol{B}_u, \quad \boldsymbol{K}_{u\alpha} = \boldsymbol{B}_u^{\mathrm{T}}\mathbb{D}\boldsymbol{B}_\alpha,$$

$$\boldsymbol{K}_{\alpha u} = \boldsymbol{K}_{u\alpha}^{\mathrm{T}}, \quad \boldsymbol{K}_{\alpha\alpha} = \boldsymbol{B}_\alpha^{\mathrm{T}}\mathbb{D}\boldsymbol{B}_\alpha$$

and

$$\mathbb{D} = \frac{\partial^2 W}{\partial\tilde{\boldsymbol{\varepsilon}}\partial\tilde{\boldsymbol{\varepsilon}}}.$$

Noting that the variations $\delta\boldsymbol{u}$ and $\delta\boldsymbol{\alpha}$ in Eq. (3.31) are arbitrary, we obtain the finite element residual vectors

$$\mathop{\mathsf{A}}_{e=1}^{nelm}\left[\boldsymbol{f}_{\mathrm{int}}(\boldsymbol{u}_e,\boldsymbol{\alpha}_e) - \boldsymbol{f}_{\mathrm{ext}}(\boldsymbol{u}_e)\right] = \boldsymbol{0} \tag{3.33a}$$

$$f_{\mathrm{enh}}(\boldsymbol{u}_e,\boldsymbol{\alpha}_e) = \boldsymbol{0}, \quad (e = 1, 2, \ldots, nelm). \tag{3.33b}$$

where

$$\boldsymbol{f}_{\mathrm{int}}(\boldsymbol{u}_e,\boldsymbol{\alpha}_e) = \int_{\Omega_e}\boldsymbol{B}_u^{\mathrm{T}}\boldsymbol{\sigma}\,\mathrm{d}V,$$
$$\boldsymbol{f}_{\mathrm{enh}}(\boldsymbol{u}_e,\boldsymbol{\alpha}_e) = \int_{\Omega_e}\boldsymbol{B}_\alpha^{\mathrm{T}}\boldsymbol{\sigma}\,\mathrm{d}V \tag{3.34}$$

$\boldsymbol{f}_{\mathrm{ext}}$ is the standard external force vector

$$\boldsymbol{f}_{\mathrm{ext}}(\hat{\boldsymbol{u}}_e) = \int_{\Omega_e}\boldsymbol{N}^{\mathrm{T}}\boldsymbol{b}\,\mathrm{d}V + \int_{\Gamma_e}\boldsymbol{N}^{\mathrm{T}}\bar{\boldsymbol{t}}\,\mathrm{d}S \tag{3.35}$$

and A is the standard finite element assembly operator. With the aid of Eq. (3.32), linearizing Eqs. (3.33a) and (3.33b) about an intermediate state $(\boldsymbol{u}_e^{(k)}, \boldsymbol{\alpha}_e^{(k)})$ yields

$$L\left[\boldsymbol{f}_{\mathrm{int}}\right] = \boldsymbol{f}_{\mathrm{int}}^{(k)} + \boldsymbol{K}_{uu}^{(k)}d\boldsymbol{u}_e + \boldsymbol{K}_{u\alpha}^{(k)}d\boldsymbol{\alpha}_e \tag{3.36a}$$

$$L\left[\boldsymbol{f}_{\mathrm{enh}}\right] = \boldsymbol{f}_{\mathrm{enh}}^{(k)} + \boldsymbol{K}_{\alpha u}^{(k)}d\boldsymbol{u}_e + \boldsymbol{K}_{\alpha\alpha}^{(k)}d\boldsymbol{\alpha}_e. \tag{3.36b}$$

From Eq. (3.33b) we observe that Eq. (3.36b) may be solved at the element level, therefore, condensing out $d\boldsymbol{\alpha}_e$

$$d\boldsymbol{\alpha}_e = -\left[\boldsymbol{K}_{\alpha\alpha}^{(k)}\right]^{-1}\left(\boldsymbol{f}_{\mathrm{enh}}^{(k)} + \boldsymbol{K}_{\alpha u}^{(k)}d\boldsymbol{u}_e\right). \tag{3.37}$$

Substituting Eq. (3.37) into Eq. (3.36a) we arrive at an equivalent displacement model involving only the nodal displacement vector at the global level

$$\boldsymbol{K}^{(k)}d\boldsymbol{u} = \boldsymbol{R}^{(k)} \tag{3.38}$$

where

$$\boldsymbol{K}^{(k)} = \mathop{\mathsf{A}}_{e=1}^{nelm}\left[\boldsymbol{K}_{uu} - \boldsymbol{K}_{u\alpha}(\boldsymbol{K}_{\alpha\alpha})^{-1}\boldsymbol{K}_{\alpha u}\right]_e^{(k)} \tag{3.39a}$$

$$\boldsymbol{R}^{(k)} = \mathop{\mathsf{A}}_{e=1}^{nelm}\left[\boldsymbol{f}^{\mathrm{ext}} - \boldsymbol{f}^{\mathrm{int}} + \boldsymbol{K}_{u\alpha}(\boldsymbol{K}_{\alpha\alpha})^{-1}\boldsymbol{f}^{\mathrm{enh}}\right]_e^{(k)}. \tag{3.39b}$$

The system (3.38) is solved and then the unknown fields are updated by

$$\boldsymbol{u}_e^{(k+1)} = \boldsymbol{u}_e^{(k)} + d\boldsymbol{u}_e \tag{3.40a}$$

$$\boldsymbol{\alpha}_e^{(k+1)} = \boldsymbol{\alpha}_e^{(k)} + d\boldsymbol{\alpha}_e. \tag{3.40b}$$

The process is repeated within a particular time step t_n until convergence of the $(k+1)$th iterate is obtained, the solution is then advanced to the next time step t_{n+1}.

Remark 3.6.

1. For linear elasticity convergence will be obtained in one iteration and the solution is then advanced to the next time increment.
2. To obtain $d\boldsymbol{\alpha}$ in Eq. (3.37) one can either recompute the array for each element for each global iterate k or store the arrays associated with the k global iterate. This storage is in addition to any other history needed for the element such as for inelasticity. For 3D problems with fine meshes the demand on memory becomes significant.
3. An alternative algorithm for obtaining the element parameters $\boldsymbol{\alpha}$ which circumvents the large demand on memory and requires storage of only the element parameters, $\boldsymbol{\alpha}$ from the previous global iterate for non-linear elasticity is given in Ref. [12].

4. Numerical simulations

In this section we investigate the performance of the proposed formulation described above. Specifically, we show the locking free response in the incompressible limit and improved performance in bending dominated problems. To assess the performance of our formulation several representative simulations are presented below in the setting of plane strain and 3D linear elasticity. Modifications to include J_2 plasticity and visco-

plasticity for physically nonlinear materials are easily included due to the strain driven format of the formulation, (see Ref. [13]). Comparisons are made with different element formulations.

The element formulations considered are:

H1 This hexahedral element is a standard eight-node displacement formulation using tri-linear interpolation functions and a standard eight-point quadrature rule, its 2D counterpart is denoted as **Q1**.

H1/E9 This hexahedral element is an enhanced formulation with nine enhanced modes and utilizes tri-linear interpolation functions and a standard eight-point quadrature rule, see Ref. [11] for further details, its 2D counterpart is denoted as **Q1/E4**.

H1/E12 This hexahedral element is an enhanced formulation with 12 enhanced modes and utilizes modified tri-linear interpolation functions and a special nine-point quadrature rule, see Ref. [12] for further details.

H1/E21 This hexahedral element is an enhanced formulation with 21 enhanced modes and utilizes tri-linear interpolation functions and a standard eight-point quadrature rule, see Ref. [1] for further details.

Shell This four-node quadrilateral shell has 6 degree-of-freedom per node and utilizes standard order quadrature, see Ref. [16] for further details.

H1/ME9 The new mixed-enhanced formulation with nine enhanced modes, standard trilinear interpolation functions, and standard eight-point quadrature rule, its 2D counterpart is denoted as **Q1/ME2**. Unless otherwise noted for the results which follow the transformation matrix, $\boldsymbol{T}$, used for the mixed-enhanced simulations was taken as the inverse transpose of the average Jacobian, i.e., $\boldsymbol{T} = \boldsymbol{J}_{\text{avg}}^{-\text{T}}$.

4.1. Eigenvalue analysis

To appraise the behavior of the elements above in the nearly incompressible limit an eigenvalue analysis for a single finite element is performed. The two configurations considered are depicted in Fig. 1. For both, the assumed mechanical properties are $E = 1$ and $\nu = 0.499999$. Tables 3 and 4 include only the 18 non-zero eigenvalues, i.e., the six rigid body modes are excluded. Values four orders of magnitude greater than the tabulated values are denoted by the ∞ symbol. For a locking-free element only one mode, corresponding to the dilatational mode, should tend toward infinity as $\nu \rightarrow 1/2$. If any additional modes tend toward infinity the element will exhibit volumetric locking.

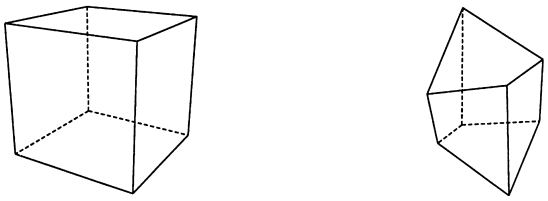

Fig. 1. Undistorted and distorted configurations of a hexahedron.

4.2. Cook's membrane problem

To demonstrate the performance of the proposed element in a bending dominated response, we consider a tapered panel clamped on one end and subjected to an in-plane shearing load on the free end, see Fig. 2. In the context of linear elasticity, this simulation is commonly referred to as Cook's membrane problem. The material properties are taken to be $E = 250$ and $\nu = 0.4999$ such that a nearly incompressible response is effectively obtained.

In Fig. 3 the top corner vertical displacement is plotted versus number of elements per side. Both the proposed Q1/ME2 element and the Q1/E4 element converge rapidly and show excellent performance, while the standard Q1 element exhibits locking behavior.

The solution time reported for both the Q1/ME2 and Q1/E4 methods were approximately the same. Also, the convergence of the Q1/ME2 with respect to the energy norm was similar to the Q1/E4.

4.3. Thick wall cylinder problem

To assess the performance of our formulation for a confined nearly incompressible state we consider a thick-walled cylindrical tube. The model consists of a 5° segment of the cylinder as depicted in Fig. 4, with an inner radius $r_{\text{i}} = 3$ and outer radius $r_{\text{o}} = 9$ subjected to an internal pressure $p = 1$. The elastic modulus was taken as $E = 1000$, while various values for Poisson's ratio are listed in Table 5. Further we assume plane strain in the axial direction. Normalized radial displacements with respect to the exact solution are found in Table 5. Both the Q1/ME2 and Q1/E4 show excellent performance, while the Q1 element locks. The same pattern with respect to solution time and convergence was observed for the present simulation as in the Cook's problem.

Table 3
Eigenvalues for a nearly incompressible eight-node regular hexahedral element

Mode	H1	H1/E9	H1/E12	H1/E21	H1/ME9
1	5.5556E−02	5.5556E−02	5.5556E−02	5.5556E−02	5.5556E−02
2	5.5556E−02	5.5556E−02	5.5556E−02	5.5556E−02	5.5556E−02
3	1.6667E−01	1.1111E−01	1.1111E−01	5.5556E−02	5.5556E−02
4	1.6667E−01	1.1111E−01	1.1111E−01	5.5556E−02	5.5556E−02
5	1.6667E−01	1.1111E−01	1.1111E−01	5.5556E−02	5.5556E−02
6	2.2222E−01	2.2222E−01	1.1111E−01	1.1111E−01	1.1111E−01
7	3.3333E−01	3.3333E−01	1.1111E−01	1.1111E−01	1.1111E−01
8	3.3333E−01	3.3333E−01	1.1111E−01	1.1111E−01	1.1111E−01
9	3.3333E−01	3.3333E−01	2.2222E−01	2.2222E−01	2.2222E−01
10	3.3333E−01	3.3333E−01	3.3333E−01	3.3333E−01	3.3333E−01
11	3.3333E−01	3.3333E−01	3.3333E−01	3.3333E−01	3.3333E−01
12	∞	3.3333E−01	3.3333E−01	3.3333E−01	3.3333E−01
13	∞	3.3333E−01	3.3333E−01	3.3333E−01	3.3333E−01
14	∞	3.3333E−01	3.3333E−01	3.3333E−01	3.3333E−01
15	∞	∞	3.3333E−01	3.3333E−01	3.3333E−01
16	∞	∞	3.3333E−01	3.3333E−01	3.3333E−01
17	∞	∞	3.3333E−01	3.3333E−01	3.3333E−01
18	∞	∞	∞	∞	∞

4.4. Thick wall sphere problem

To demonstrate the performance of our 3D formulation for a nearly incompressible state in a 3D stress state we consider a thick-walled sphere depicted in Fig. 5 with an inner radius $r_i = 7.5$ and outer radius $r_o = 10$ subjected to an internal pressure $p = 1$. The elastic modulus was taken as $E = 250$, while various values for Poisson's ratio are listed in Table 6. Normalized radial displacements with respect to the exact solution are found in Table 6. The H1/ME9 element shows excellent performance, while the H1 element performance is poor and locks. Again the same pattern with respect to solution time and convergence as reported in the previous problems was observed for the present simulation.

Table 4
Eigenvalues for nearly incompressible eight-node distorted hexahedral element

Mode	H1	H1/E9	H1/E12	H1/ME9
1	3.6273E−02	3.0720E−02	3.3857E−02	3.3108E−02
2	7.5142E−02	5.5337E−02	5.6785E−02	3.9517E−02
3	1.3489E−01	1.0233E−01	8.0446E−02	6.6768E−02
4	1.6698E−01	1.3401E−01	1.0274E−01	7.4400E−02
5	1.9041E−01	1.4662E−01	1.0760E−01	8.2449E−02
6	2.1365E−01	1.9201E−01	1.2176E−01	8.9910E−02
7	2.5897E−01	2.1791E−01	1.3636E−01	1.0429E−01
8	3.2395E−01	2.5554E−01	1.4528E−01	1.5998E−01
9	3.8442E−01	2.9852E−01	1.8486E−01	1.7127E−01
10	4.0333E−01	3.1738E−01	2.3426E−01	2.2994E−01
11	2.1370E+01	3.8075E−01	2.6414E−01	2.6744E−01
12	∞	4.3302E−01	2.9215E−01	3.0429E−01
13	∞	4.8680E−01	3.4335E−01	3.1834E−01
14	∞	3.8748E+01	3.7548E−01	3.4756E−01
15	∞	∞	3.8995E−01	4.2667E−01
16	∞	∞	4.6811E−01	4.4534E−01
17	∞	∞	5.2791E−01	5.0957E−01
18	∞	∞	∞	∞

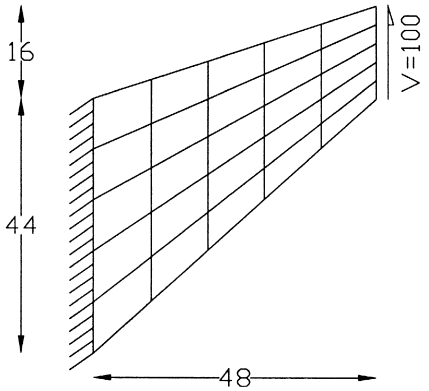

Fig. 2. Cook's membrane problem.

4.5. 2D limit analysis

To appraise the behavior of the elements above in a highly constrained elastoplastic problem, we introduce the double notched specimen after Nagtegaal et al. [7]. This simulation produces a limit load in terms of the net stress given analytically by $\sigma_{lim} = (2+$

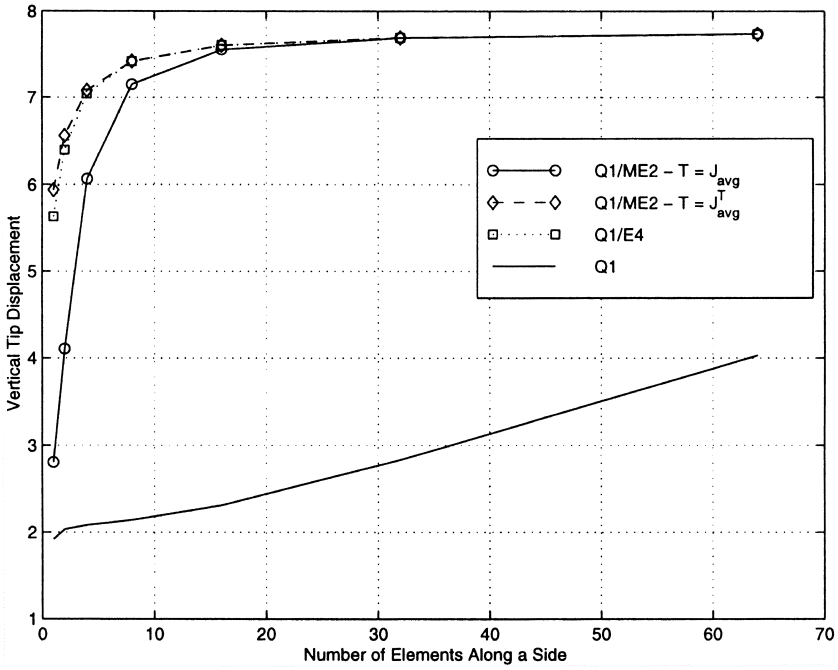

Fig. 3. Convergence of the finite element solutions for Cook's problem.

$\pi)\sigma_y/\sqrt{(3)} \approx 2.97$. The material parameters used for the elastic-perfectly plastic plane strain simulation are: $E = 70$, $\nu = 0.3$ and $\sigma_y = 1.0$, while the geometric properties are: $H = 30$, $W = 10$ and $b = 1$. Due to symmetry only one-quarter of the geometry was analyzed with the resultant mesh being 15×5. The loading was simulated via displacement control at the end opposite the ligament. Thirty displacement increments were chosen for the simulation. Results in Fig. 6 show that the standard displacement formulation does not obtain the limit load, but instead increases monotonically with increased load, whereas the proposed mixed-enhanced formulation asymptotes to near the analytical solution.

4.6. 3D limit analysis

To appraise the 3D behavior of the elements above in a highly constrained elastoplastic problem, we introduce the 3D rectangular block after Andelfinger et al. [1]. The material parameters used for the elastic–plastic simulation are: $E = 210{,}000$, $\nu = 0.3$, $H_{\text{iso}} = 210$, $H_{\text{kin}} = 0$ and $\sigma_y = 250$, while the geometric properties are: $H = 50$, $W = 100$ and $L = 100$. Due to symmetry only one-quarter of the geometry was analyzed with the resultant mesh being $5 \times 5 \times 5$. The loading was simulated via displacement control at the central patch on the mesh, as depicted in Fig. 7. Thirty displacement increments were chosen for the simulation. Results in Fig. 8 show that the standard displacement formulation does not obtain the limit load, but instead increases monotonically with increased load, whereas the proposed mixed-enhanced formulation asymptotes to the slope of the hardening parameter, H_{iso}.

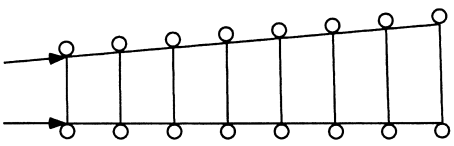

Fig. 4. Thick wall cylinder problem.

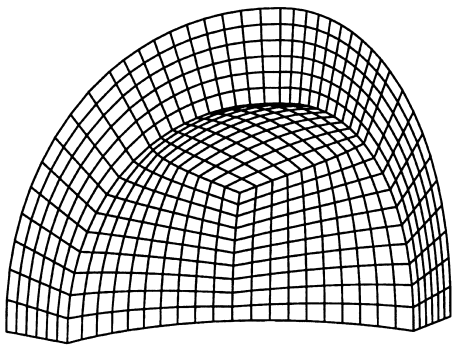

Fig. 5. Thick wall sphere problem.

Table 5
Normalized radial displacement at $r = 3$

ν	Q1	Q1/E4	Q1/ME2 ($\boldsymbol{T} = \boldsymbol{J}_{\text{avg}}$)	Q1/ME2 ($\boldsymbol{T} = \boldsymbol{J}^{\text{T}}_{\text{avg}}$)
0.00000	0.997	0.998	1.000	0.997
0.25000	0.985	0.986	0.989	0.987
0.30000	0.980	0.982	0.985	0.981
0.49000	0.884	0.960	0.964	0.960
0.49900	0.505	0.959	0.962	0.959
0.49990	0.096	0.959	0.962	0.958
0.49999	0.011	0.959	0.962	0.958

Table 6
Normalized radial displacement at $r = 10$

ν	H1	H1/E9	H1/ME9
0.49000	0.992	1.018	1.019
0.49900	0.772	0.998	1.001
0.49990	0.250	0.985	0.999
0.49999	0.033	0.936	0.999

4.7. Viscoplasticity

We consider a perforated strip shown in Fig. 9 illustrating the behavior of the formulation when subject to a viscoplastic response [8]. The material parameters used for the elastic–viscoplastic plane strain simulations are: $E = 70$, $\nu = 0.3$, $\sigma_y = 0.243$, $H_{\text{iso}} = 0.135$ and $H_{\text{kin}} = 0.015$, while the geometric properties are: $H = 36$, $W = 10$ and $R = 5$ after an example in Ref. [22]. Due to symmetry only one-quarter of the geometry was analyzed. The loading was simulated via displacement control at the end opposite the ligament. Fifteen displacement increments were chosen for the simulation. Results in Fig. 9 shows the results for various values of viscosity as well as the elasticity and rate independent plasticity solution.

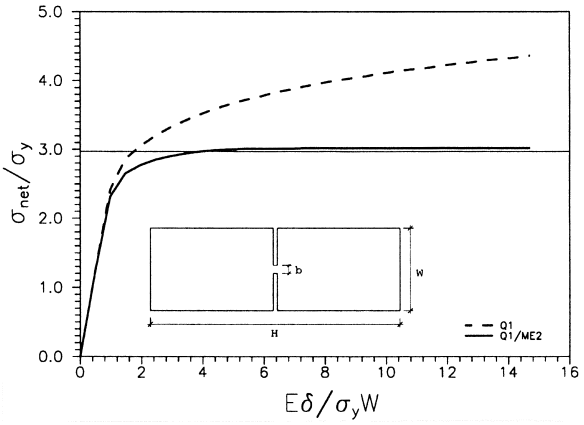

Fig. 6. Notched tensile specimen: limit analysis.

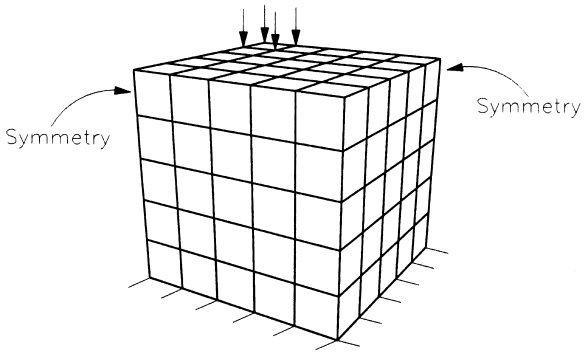

Fig. 7. Elasto-plastic rectangular block.

4.8. Pinched cylindrical shell with end diaphragm

To demonstrate the performance of our 3D formulation for singly curved thin shell structures we examine a pinched cylindrical shell with end diaphragm proposed by MacNeal and Harder [6]. We consider the configuration of the cylindrical shell as depicted in Fig. 10 with an inner radius $r_{\text{i}} = 300$, wall thickness $t = 3.0$ and length $L = 600$. The elastic modulus was taken as $E = 3.0 \times 10^6$ and a Poisson's ratio of $\nu = 0.3$. One-eighth of the shell is modeled by an $N \times N$ mesh defined in cylindrical coordinates. Results reported in Table 7 for the vertical displacement under the load are normalized with respect to the reference value 1.82488×10^5. The H1/ME9 element shows excellent performance for the thin shell limit.

4.9. Pinched spherical hemisphere

To demonstrate the performance of our 3D formu-

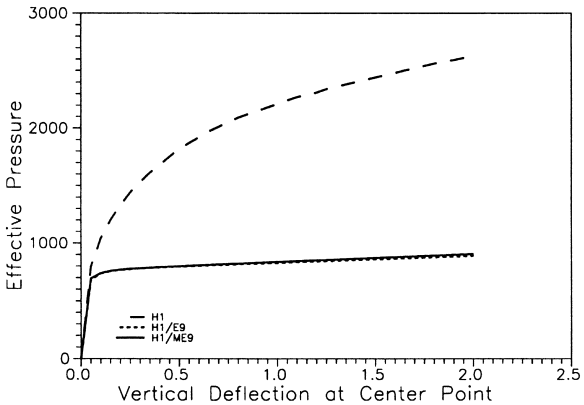

Fig. 8. Load-deflection curves for an elasto-plastic rectangular block.

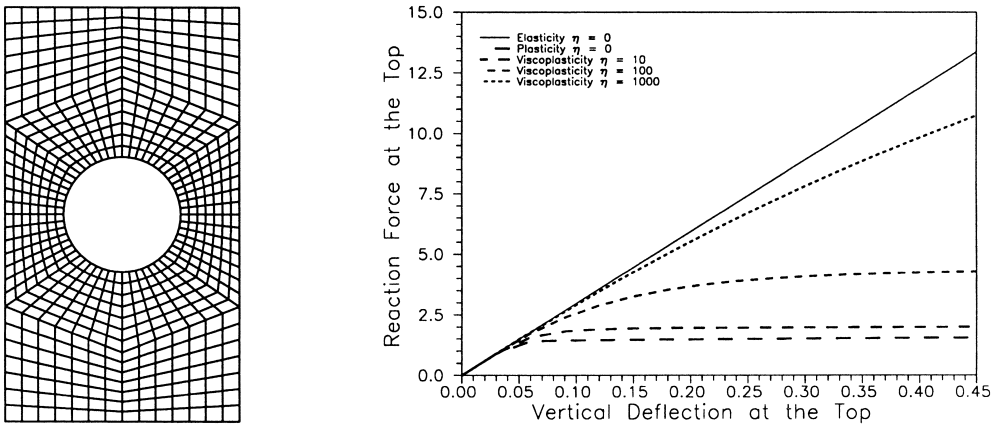

Fig. 9. Perforated strip at various viscosities.

lation for doubly curved thin shell structures we examine a pinched hemisphere with an open top, modeled as an 18° spherical cap as proposed by MacNeal and Harder [6]. We consider the configuration of the spherical shell as depicted in Fig. 11 with an inner radius $r_i = 10$ and wall thickness $t = 0.04$. The elastic modulus was taken as $E = 6.825 \times 10^7$ and a Poisson's ratio of $\nu = 0.3$. One-quarter of the shell is modeled by an $N \times N$ mesh defined in spherical coordinates. Results reported in Table 8 for the displacement under the load are normalized with respect to the reference value 0.094. The H1/ME9 element shows excellent performance for the thin shell limit.

5. Closure

We have presented a preliminary investigation for a new class of *assumed strain* methods employing low order finite elements in the setting of physically nonlinear elasticity. The present methodology circumvents difficulties in stress recovery in additional to improved coarse mesh accuracy and locking free response in quasi-incompressible regimes. The formulation exhibits favorable performance in comparison to the Q1/E4 element, which is currently a widely used element.

From the numerical simulations presented, several noteworthy characteristics have been found:

1. In bending dominated response coarse mesh accuracy is favorable. Improvements to bending dominate regimes may result if: (a) introduce alternative enhanced modes, (b) introduce alternative procedures for transforming the isoparametric stress and strain interpolates to the reference configuration. One such alternative would be to modify the original reference coordinate system used to compute $\boldsymbol{T}$ by simply rotating the physical element to align equally with the isoparametric coordinate system, while maintaining the aspect ratio. The new coordinate frame is then used to form the average Jacobian. This modified Jacobian has two features: (i) the proposed Jacobian removes any element dis-

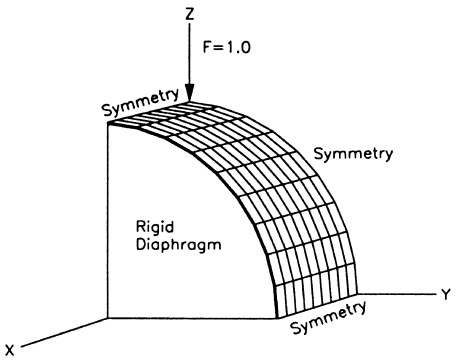

Fig. 10. Pinched cylindrical shell problem.

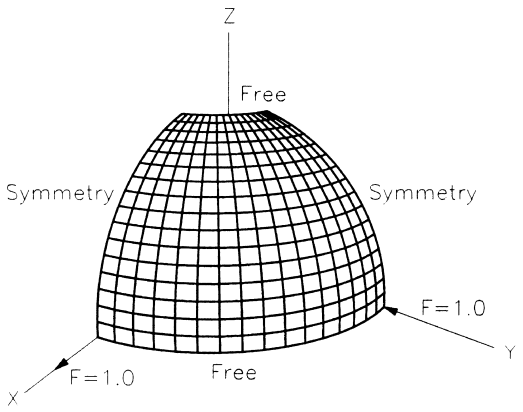

Fig. 11. Pinched spherical hemisphere.

Table 7
Normalized displacement under the load

Mesh	H1	Shell	H1/E9	H1/ME9
$4 \times 4 \times 1$	0.035	0.636	0.081	0.107
$8 \times 8 \times 1$	0.069	0.951	0.405	0.496
$16 \times 16 \times 1$	0.148	1.016	0.838	0.914
$16 \times 16 \times 2$	0.149	–	0.835	0.908
$16 \times 16 \times 3$	0.149	–	0.834	0.907
$32 \times 32 \times 1$	0.315	–	0.976	0.992

Table 8
Normalized displacement under the load

Mesh	H1	Shell	H1/E9	H1/ME9
$4 \times 4 \times 1$	0.001	0.897	0.010	0.039
$8 \times 8 \times 1$	0.003	0.999	0.163	0.732
$16 \times 16 \times 1$	0.010	0.995	0.780	0.989
$16 \times 16 \times 2$	0.010	–	0.782	0.988
$16 \times 16 \times 3$	0.010	–	0.749	0.988
$32 \times 32 \times 1$	0.039	0.994	0.974	0.998

tortion, and (ii) the resulting Jacobian is diagonal yielding additional efficiency for the computation of arrays. Both classes of improvements need to be pursued in future work.

2. The orthogonality condition which arises between the stress and enhanced strain field in many *assumed strain* formulations, does not explicitly appear in the present work, hence, variationally consistent stress is permissible.
3. Since the mixed parameters, $\boldsymbol{\gamma}$ may be computed explicitly the resulting element is efficient and retains standard quadrature order to exactly integrate arrays, unlike most enhanced strain formulations.
4. The element exhibits favorable behavior for configurations where element aspect ratios are large, such as thin shell like structure.
5. Since the element uses strain driven constitutive relations in the formulation extension to nonlinear constitutive relations is easily obtainable as demonstrated with the implementation of rate dependent and independent plasticity.

The preliminary performance exhibited by the Q1/ME2 and Q1/ME9 in bending and quasi-incompressible regions offers an attractive methodology for a systematic development of mixed-enhanced finite elements. Extension to the finite deformation case is presented in Part 2 of this paper.

Appendix A

To allow for general mappings $\mathscr{E}_1$ and $\mathscr{E}_2$ which retain the orthogonality property

$$\int_{\square} \mathscr{E}_1(\cdot)\mathscr{E}_2(\cdot)\,\mathrm{d}\square = 0 \tag{A1}$$

we introduce the following transformation

$$\bar{\mathscr{E}}_2(\boldsymbol{\alpha}) = \mathscr{E}_2(\boldsymbol{\alpha}) - \mathscr{E}_1(\boldsymbol{\gamma})\boldsymbol{H}_\gamma^{-1}\boldsymbol{H}_\alpha \tag{A2}$$

where

$$\boldsymbol{H}_\gamma = \int_\Omega \mathscr{E}_1^{\mathrm{T}}(\delta\boldsymbol{\beta})\mathscr{E}_1(\boldsymbol{\gamma})\,\mathrm{d}V \quad \text{and}$$
$$\boldsymbol{H}_\alpha = \int_\Omega \mathscr{E}_1^{\mathrm{T}}(\delta\boldsymbol{\beta})\mathscr{E}_2(\boldsymbol{\gamma})\,\mathrm{d}V. \tag{A3}$$

Note that the above transformation does not guarantee

$$\int_{\square} \mathscr{E}_1(\cdot)\,\mathrm{d}\square \quad \text{and} \quad \int_{\square} \mathscr{E}_2(\cdot)\,\mathrm{d}\square = 0 \tag{A4}$$

which allows the element parameters to be easily decoupled. To ensure the resulting arrays are not singular the choice of $\mathscr{E}_1$ and $\mathscr{E}_2$ is such that their columns are linearly independent (i.e. $\boldsymbol{H}_\gamma^{-1}$ exists).

References

[1] Andelfinger U, Ramm E, Roehl D. 2D- and 3D-enhanced assumed strain elements and their application in plasticity. In: Owen D, Onate E, Hinton E, editors. Computational Plasticity, Proceedings of the Fourth International Conference. Swansea, UK: Pineridge, 1992. p. 1997–2007.

[2] Glaser S, Armero F. On the formulation of enhanced strain finite elements in finite deformations. Engineering Computations 1997;14:759–91, in press.

[3] Hughes TRJ. The finite element method. Englewood Cliff, NJ: Prentice-Hall, 1987.

[4] Korelc J, Wriggers P. An efficient 3D enhanced strain element with Taylor expansion of the shape functions. Computational Mechanics 1996;19:30–40.

[5] Korelc J, Wriggers P. Improved enhanced strain four-node element with Taylor expansion of the shape functions. International Journal of Numerical Methods in Engineering 1997;40:407–21.

[6] MacNeal RH, Harder RL. A proposed standard set of problems to test finite element accuracy. Journal of Finite Elements in Analysis and Design 1985;1:3–20.

[7] Nagtegall JC, Parks DM, Rice JR. On numerical accurate finite element solutions in the fully plastic range. Computer Methods in Applied Mechanics and Engineering 1974;4:153–77.

[8] Perzyna P. Fundamental problems in viscoplasticity. Advances in Applied Mechanics 1966;9:243–377.
[9] Pian THH, Sumihara K. Rational approach for assumed stress finite elements. International Journal of Numerical Methods in Engineering 1985;20:1685–95.
[10] Simo JC, Rifai MS. A class of mixed assumed strain methods and the method of incompatible modes. International Journal of Numerical Methods in Engineering 1990;29:1595–638.
[11] Simo JC, Armero F. Geometrically non-linear enhanced strain mixed methods and the method of incompatible modes. International Journal of Numerical Methods in Engineering 1992;33:1413–49.
[12] Simo JC, Armero F, Taylor RL. Improved versions of assumed enhanced strain tri-linear elements for 3D finite deformation problems. Computer Methods in Applied Mechanics and Engineering 1993;110:359–86.
[13] Simo JC, Hughes TJR. Computational inelasticity. New York: Springer, 1998.
[14] Sokolnikoff IS. Tensor analysis theory and applications to geometry and mechanics of continua. New York: Wiley, 1964.
[15] Taylor RL, Beresford PJ, Wilson EL. A non-conforming element for stress analysis. International Journal of Numerical Methods in Engineering 1976;10:1211–9.
[16] Taylor RL. Finite element analysis of linear shell problems. In: Whiteman JR, editor. The mathematics of finite elements and applications VI, MAFELAP. London: Academic Press, 1987.
[17] Washizu K. Variational methods in elasticity and plasticity, 3rd ed. New York: Pergamon Press, 1982.
[18] Weissman SL. High-accuracy low-order three-dimensional brick elements. International Journal of Numerical Methods in Engineering 1996;39:2337–61.
[19] Wilson EL, Taylor RL, Doherty WP, Ghaboussi J. Incompatible displacement models. In: Fenves SJ, Perrone N, Robinson AR, Schnobrich WC, editors. Numerical and Computer Methods in Structural Mechanics. New York: Academic Press, 1973. p. 43–57 .
[20] Wriggers P, Reese S. A note on enhanced strain methods for large deformations. Computer Methods in Applied Mechanics and Engineering 1996;135:201–9.
[21] Zienkiewicz OC, Taylor RL. In: The finite element method, vol. 1. New York: McGraw-Hill, 1989 4th ed.
[22] Zienkiewicz OC, Taylor RL. In: The finite element method, vol. 2. New York: McGraw-Hill, 1991 4th ed.